*34th EPS Conference on Plasma Phys. Warsaw, 2 - 6 July 2007 ECA Vol.**31F**, P-4.031 (2007)*

Paleoclassical Model For Electron Temperature Pedestal*

J.D. Callen, *University of Wisconsin, Madison, WI 53706-1609 USA*
T.H. Osborne, R.J. Groebner, H.E. St. John,
General Atomics, San Diego, CA, 92186-5608 USA
A.Y. Pankin, G. Bateman, A.H. Kritz, K. McFarland,
Lehigh University, Bethlehem, PA 18015-3182 USA
W.M. Stacey, *Georgia Tech, Atlanta, GA 30332 USA*

Context. At the recent IAEA Chengdu meeting, the paleoclassical model [1] of radial electron heat transport was shown to compare favorably [2] with mostly ohmic-level transport analysis data from a number of toroidal plasma experiments and set the lower limit (factor ~ 2 in tokamak plasmas) on electron heat transport. Anomalous transport induced by drift-wave-type microturbulence usually scales with the gyroBohm coefficient $D^{\rm gB} \equiv (\varrho_S/\bar{a})(T_e/eB) \propto T_e^{3/2}/\bar{a}B^2$ and hence could become small in the edge region where T_e is low and in H-mode pedestals where the fluctuation level is usually reduced. In contrast, for the recently developed paleoclassical transport model [1] the electron heat diffusivity $\chi_e^{\rm pc} \propto \bar{a}^{1/2}T_e^{-3/2}$ increases as the electron temperature decreases toward the plasma edge and divertor separatrix. Thus, we can anticipate [2] that for $T_e \lesssim T_e^{\rm crit} \simeq B({\rm T})^{2/3}\bar{a}({\rm m})^{1/2}$ keV ($\sim$ 0.6–2.4 keV in present plasmas, but $\sim$ 3.5–5 keV in ITER) paleoclassical radial electron heat transport could be dominant. In particular, it could be dominant in the pedestal of H-mode plasmas.

Model Assumptions. Key model assumptions for developing a model [3] for the T_e H-mode pedestal based on paleoclassical electron heat transport are: 1) In a "near transport equilibrium" state between Type I (large, long repetition time) ELMs, electron heat transport is dominated by paleoclassical radial electron heat transport [1] in the edge pedestal. 2) The electron temperature on the divertor separatrix is fixed [4] — by balancing heat flow across the separatrix against parallel electron heat conduction on open field lines outside it. And 3) the edge electron density profile is fixed, and in particular given by the hyperbolic tangent form proposed by Porter *et al.* [4] whose characteristic width is Δ_n [5,6] (typically $\sim$ cm) and whose radial position of the inflection point in the edge density profile (where $|\boldsymbol{\nabla} n_e|$ is maximum) is ρ_n — see Fig. 1.

Paleoclassical Model. The equiliibrium electron energy balance is thus [1b,1c]

$$Q_e = \frac{\partial}{\partial V}\langle \mathbf{Q}_e^{\rm pc}\cdot\boldsymbol{\nabla} V\rangle \equiv -\frac{M+1}{V'}\frac{d^2}{d\rho^2}\left(V'\frac{D_\eta}{\bar{a}^2}\frac{3}{2}n_eT_e\right). \qquad (1)$$

Here, Q_e is the net electron heating power per unit volume (direct heating plus collisional heating from ions minus convection and radiation losses) and $\langle \mathbf{Q}_e^{\rm pc}\cdot\boldsymbol{\nabla} V\rangle$ is the radial electron heat flow induced in resistive, current-carrying toroidal plasmas by the paleoclassical processes [1c,1d,2] of electron guiding centers and heat being transported along with thin poloidal flux annuli diffusing radially with the magnetic field diffusivity $D_\eta \equiv \eta_\parallel^{\rm nc}/\mu_0$:

$$\chi_e^{\rm pc} \simeq \frac{3}{2}(M+1)D_\eta,\ \ D_\eta \simeq \frac{\eta_\parallel^{\rm nc}}{\eta_0}\,\frac{1400\,Z}{[T_e({\rm eV})]^{3/2}}\,\frac{\rm m^2}{\rm s}, \qquad (2)$$

where $Z \to Z_{\rm eff} \equiv \sum_i n_iZ_i^2/n_e$. The ratio of neoclassical parallel resistivity $\eta_\parallel^{\rm nc}$ to reference (perpendicular) resistivity $\eta_0 \equiv m_e\nu_e/n_ee^2 \simeq 1400\,Z/[T_e({\rm eV})]^{3/2}$ is approximately [1b,1c] $\eta_\parallel^{\rm nc}/\eta_0 \simeq 0.43 + 2\,/\,(1+\nu_{*e}^{1/2}+\nu_{*e})$ for DIII-D edge plasmas where $Z_{\rm eff} \sim$ 2–2.5. Here, $\nu_{*e} \equiv R_0q/(\epsilon^{3/2}\lambda_e)$ is the neoclassical electron collisionality parameter with electron collision

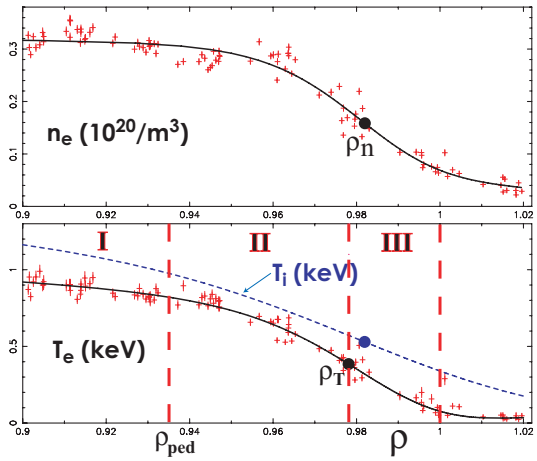

Figure 1: "Equilibrium" n_e, T_e pedestal profiles for DIII-D H-mode shot 98889, averaged over 80–99% of time ($\sim$ 36 ms) to next ELM crash, around 4500 ms. The lines show tanh fits to Thomson scattering data with symmetry points at ρ_n, ρ_T.

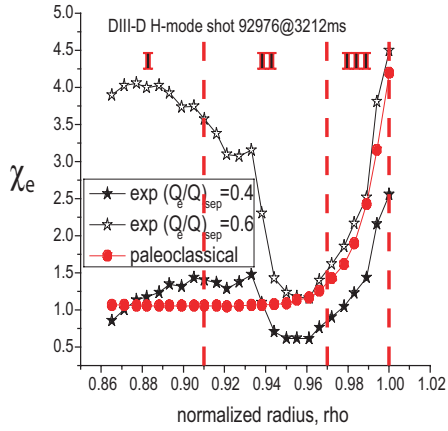

Figure 2: Interpretive [7a] profile of χ_e, $\chi_e^{\rm pc}$ (m^2/s) in pedestal similar to Fig. 1. Agreement in edge (II,III) is reasonable since uncertainties in both χ_e values are $\gtrsim 2$. Here, $(Q_E/Q)_{\rm sep}$ is assumed electron fraction of power flow through the separatrix.

length $\lambda_e \simeq 1.2\times 10^{16}[T_e({\rm eV})]^2/(n_e Z)$ m and $\epsilon \equiv r/R_0 \simeq 0.4$ is the DIII-D edge inverse aspect ratio. For edge plasmas the paleoclassical helical multiplier M is [1b,1c,2]

$$M \simeq \frac{1}{\pi \bar{R} q\,/\lambda_e + 1/n_{\rm max}}, \quad n_{\rm max} \equiv \frac{1}{(\pi \bar{\delta}_e q')^{1/2}}, \tag{3}$$

in which $\bar{R} \simeq R_0$ is an average major radius, $\bar{\delta}_e \equiv (c/\omega_p \bar{a})$ is a dimensionless electromagnetic skin depth and $q' \equiv |dq/d\rho|$. Also, ρ is a toroidal-flux-based dimensionless radial variable, $V' \equiv dV/d\rho \propto \rho$ is the radial derivative of the volume of a flux surface, and $\bar{a} \simeq a\,[2\kappa^2/(1+\kappa^2)]^{1/2}$ is a (paleoclassical) average radius for a plasma with nominal minor radius a and ellipticity $\kappa = b/a$. Symbols in (1)–(3) are defined precisely in [1b,1c].

Pedestal Characteristics, Regions. Figure 1 shows typical "equilibrium" electron density and temperature profiles in a DIII-D low density H-mode pedestal. As indicated, the T_e profile will be characterized by three regions [3]: III (bottom half of pedestal, $\rho_T < \rho < 1$), from separatrix inward to the T_e inflection point $\rho_T \simeq 0.978$; II (top half of pedestal, $\rho_{\rm ped} < \rho < \rho_T$), from T_e inflection point to top of T_e pedestal defined here as the point $\rho_{\rm ped} \simeq \rho_T - 2\Delta_T \simeq 0.935$ where $\tanh 2 \simeq 0.964$; and III (core, $\rho < \rho_{\rm ped}$), from top of T_e pedestal inward to the hot core plasma.

Transport Modeling. The "power balance" electron heat diffusivity χ_e obtained from interpretive transport modeling [7a] is compared with the $\chi_e^{\rm pc}$ defined in (2)–(3) in Fig. 2. Other DIII-D discharge comparisons [7b,8] show similar agreement but often with somewhat larger differences in the region of minimum χ_e. Figure 3 shows predictive modeling of the edge T_e profile for 98889-type discharge parameters using the ASTRA code [9]; it shows that the transition from region II to I is where anomalous diffusion induced by microturbulence becomes a significant fraction ($> 20\%$) of the paleoclassical $\chi_e^{\rm pc}$. Similar χ_e profiles for other H-mode pedestals that increase strongly toward the separatrix are shown in [7,8,10]; χ_e and $\chi_e^{\rm pc}$ agree in most but not all "equilibrium" cases in regions II (partially) and III (mostly). Paleoclassical transport predictions for pedestal $T_e(\rho)$ and $T_e^{\rm ped}$ in the three regions will now be discussed.

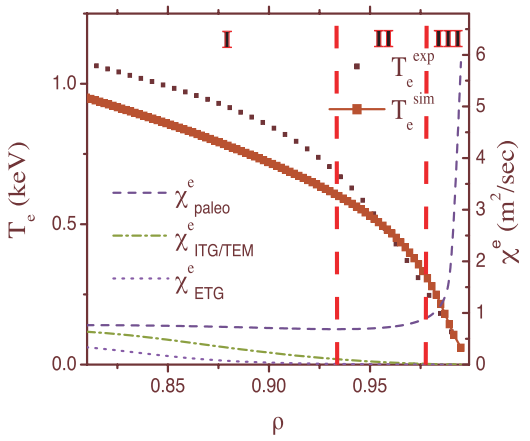

Figure 3: ASTRA modeling [9] of $T_e(\rho)$ in H-mode pedestal in Fig. 1. Diffusivities due to ion-temperature-gradient/trapped-electron and electron-temperature-gradient microinstabilities are $\chi^e_{\rm ITG/TEM}$ and $\chi^e_{\rm ETG}$.

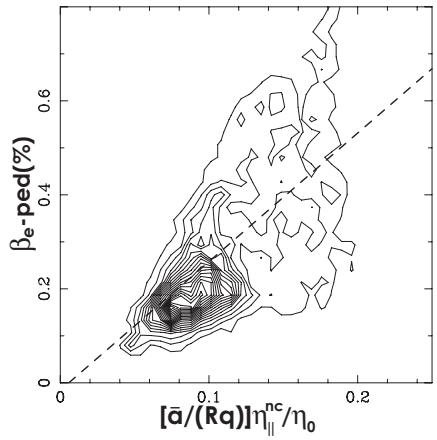

Figure 4: Probability contours from DIII-D pedestal database "between ELM crashes" shows $\beta_e^{\rm ped}$ agrees approximately with prediction in (4). Dashed line is linear fit to data.

Region III: Inside but near the magnetic separatrix in diverted plasmas q becomes very large and the paleoclassical helical multiplier M becomes unity or less. At ρ_T in Fig. 1, $M \simeq 1.8$; but $M \propto T_e^2/n_e q$ decreases rapidly for $\rho > \rho_T$ and $M < 1$ for $\rho \gtrsim 0.985$. In this region ν_{*e} is large and the neoclassical resistivity reduces to the Spitzer resistivity $\eta_\parallel^{\rm Sp}$. Thus, close to the separatrix the paleoclassical electron heat diffusivity becomes [1b,1c,2] $\chi_{es}^{\rm pc} \simeq (3/2)\,\eta_\parallel^{\rm Sp}/\mu_0 \simeq 900\,Z/[T_e({\rm eV})]^{3/2}$ m^2/s. Since $\chi_e \simeq \chi_e^{\rm pc}$ decreases as T_e increases inside the separatrix, we infer from a Fourier heat flux relation $\mathbf{q}_e \simeq -\,n_e\chi_e\boldsymbol{\nabla}T_e$ that $|\boldsymbol{\nabla}T_e|$ should increase for decreasing ρ. Thus, in region III $T_e(\rho)$ should have positive or neutral curvature ($d^2T_e/d\rho^2 \geq 0$), as is evident in Fig. 1 and is usually observed experimentally in H-mode plasmas. The rapid increase of $\chi_e^{\rm pc}$ with ρ is critical for obtaining $\partial^2 T_e/\partial\rho^2 \geq 0$ in this region, as indicated in Fig. 3. Integrating (1) twice from the separatrix inward over the volume of the radial (ρ) region where $M << 1$ and neglecting local electron heating, it can be shown [3] that T_e is predicted to scale like n_e^2 — to keep the electron heat flow nearly constant through region III. This prediction agrees with H-mode pedestal data from ASDEX-Upgrade [10,11]; it also predicts [11] that in region III the ratio of electron temperature gradient to electron density gradient $\eta_e \equiv d\ln T_e/\,d\ln n_e \simeq 2$. Studies based on the ratio of the density to temperature gradient scale lengths at the symmetry point ρ_T of the pedestal T_e profile tanh fit found $\eta_e \sim 1$–3 in DIII-D [12].

Region II. Inside the inflection point $\rho = \rho_T$ the helical multiplier $M \simeq \lambda_e/\pi\bar{R}q$ is usually greater than unity and the effective paleoclassical electron heat diffusivity is in its collisional (Alcator scaling) regime where: $\chi_{e\rm II}^{\rm pc} \simeq (3/2)(\eta_\parallel^{\rm nc}/\eta_0)(v_{Te}/\pi\bar{R}q)(c^2/\omega_p^2)$. Moving inward from the inflection point (ρ_T), the effective $\chi_e^{\rm pc} \propto T_e^{1/2}/n_e q$ decreases slowly, as indicated in Figs. 2 and 3. This causes $|\boldsymbol{\nabla}T_e|$ to decrease [7] as we move inside ρ_T — because in moving inward n_e is increasing and the electron heat flow $\langle\mathbf{q}_e\cdot\boldsymbol{\nabla}V\rangle$ is decreasing. There is no simple way to estimate the T_e profile in region II.

Pedestal Height. Because microturbulence-induced transport typically dominates in the hot core plasma and has a threshold-type behavior, whereas paleoclassical transport

may dominate in the edge, varies smoothly and decreases as we move into the hot core, we hypothesize that the pedestal height is determined by the transition (at $\rho \sim 0.85$ in Fig. 3) between these two transport processes. Presuming paleoclassical transport is in its collisional regime ($\chi_{eII}^{\rm pc}$), the pedestal electron pressure can be estimated [3] by equating $\chi_{eII}^{\rm pc}$ to an anomalous $\chi_e^{\rm gB} \equiv f_\# D^{\rm gB}$ with an order unity, threshold-type dimensionless coefficient $f_\#$ that depends on many local quantities (magnetic shear, T_e/T_i, ν_{*e} etc.):

$$p_e^{\rm ped} \equiv n_e^{\rm ped} T_e^{\rm ped} \simeq \frac{0.032}{f_\# A_1^{1/2}} \frac{\bar{a}}{\bar{R}q} \frac{\eta_\parallel^{\rm nc}}{\eta_0} \frac{B^2}{2\mu_0} \propto B_p B. \tag{4}$$

This relation yields $\beta_e^{\rm ped} \simeq (0.023/f_\#)(\bar{a}/R_0 q)(\eta_\parallel^{\rm nc}/\eta_0)$ for deuterium ($A_i = 2$). Figure 4 shows this prediction is reasonably consistent with the DIII-D pedestal database in both scaling ($f_\# \simeq 0.82$ for slope of fitted data in Fig. 4) and magnitude ($0.6 \lesssim f_\# \lesssim 2$).

Region I. In the hot core, paleoclassical transport is mostly in its collisionless regime ($\lambda_e > \pi \bar{R} q n_{\rm max}$) where $\chi_{eI}^{\rm pc} \simeq (3/2) n_{\rm max} D_\eta$. However, since $T_e \gtrsim T_e^{\rm crit} \simeq B^{2/3} \bar{a}^{1/2} (3 f_\#)^{-1/3}$ keV [2,3] (~ 1 keV using $f_\# \simeq 0.82$ from Fig. 4 for the DIII-D shot in Fig. 1) there, anomalous electron heat transport due to microturbulence usually dominates over paleoclassical transport in region I (i.e., for $\rho < 0.85$ in Fig. 3). (In ITER, $T_e^{\rm crit} \sim 3.5$–5 keV.)

Conclusion. The paleoclassical model for H-mode T_e pedestals [3] compares well with DIII-D data in three important regards: 1) $\chi_e^{\rm pc}(\rho)$ and modeled $T_e(\rho)$ in regions III and (less so) II, 2) positive or neutral T_e profile curvature and $\eta_e \simeq 2$ in region III, and 3) $\beta_e^{\rm ped}$ prediction from (4) due to change from collisional paleoclassical to microturbulence-induced anomalous transport near transition from region II to I. Similar tests on pedestals in other H-mode tokamak plasmas are needed to determine how limited or universal these conclusions are, and perhaps to separate effects of paleoclassical transport and peeling-ballooning instabilities (ELMs) whose scalings are quite similar.

*Research supported by U.S. DoE grants & contracts DE-FG02-92ER54139 (UW-Madison), DE-FC02-04ER54698 (GA), DE-FG02-92ER54141 (Lehigh), and DE-FG02-00ER54538 (GaTech).

[1] J.D. Callen, a) Phys. Rev. Lett. **94**, 055002 (2005); b) Phys. Plasmas **12**, 092512 (2005); c) Nucl. Fusion **45**, 1120 (2005); and d) Phys. Plasmas **14**, 040701 (2007). References [1]–[3] are all available from `http://homepages.cae.wisc.edu/~callen`.

[2] J.D. Callen, J.K. Anderson, T.C. Arlen, G. Bateman, R.V. Budny, T. Fujita, C.M. Greenfield, M. Greenwald, R.J. Groebner, D.N. Hill, G.M.D. Hogeweij, S.M. Kaye, A.H. Kritz, E.A. Lazarus, A.C. Leonard, M.A. Mahdavi, H.S. McLean, T.H. Osborne, A.Y. Pankin, C.C. Petty, J.S. Sarff, H.E. St. John, W.M. Stacey, D. Stutman, E.J. Synakowski, K. Tritz, "Experimental Tests of Paleoclassical Transport," paper EX/P3-2, 2006 IAEA Fus. Energy Conf., Chengdu, China: http://www-pub.iaea.org/MTCD/Meetings/fec2006pp.asp (UW-CPTC 06-5, to be published).

[3] J.D. Callen, T.H. Osborne, R.J. Groebner, H.E. St. John, A.Y. Pankin, G. Bateman, A.H. Kritz, W.M. Stacey, "Paleoclassical model for electron temperature pedestal," UW-CPTC 06-6, March 2007 (to be published).

[4] G.D. Porter *et al.*, Phys. Plasmas **5**, 1410 (1998).

[5] M.A. Mahdavi *et al.*, Nucl. Fusion **42**, 52 (2002).

[6] R.J. Groebner *et al.*, Nucl. Fusion **44**, 204 (2004).

[7] W.M. Stacey and R.J. Groebner, a) Phys. Plasmas **13**; b) 072510 (2006); **14**, 012501 (2007).

[8] W.M. Stacey and T.E. Evans, Phys. Plasmas **13**, 112506 (2006).

[9] A.Y. Pankin, G. Bateman, D.P. Brennan, D.D. Schnack *et al.*, Nucl. Fusion **46**, 403 (2006).

[10] L.D. Horton *et al.*, Nucl. Fusion **45**, 856 (2005) — see Figs. 2, 3.

[11] J. Neuhauser *et al.*, Plasma Phys. Control. Fusion **44**, 855 (2002) — see Fig. 5.

[12] R.J. Groebner *et al.*, Plasma Phys. Control. Fusion **48**, A109 (2006) — see Fig. 3b.